Verification of the Thermal Module in the ELESIM Code and the Associated Uncertainty Analysis

by

V.I. Arimescu, A.F. Williams, M.E. Klein W.R. Richmond and M. Couture

1. Introduction

Temperature is a critical parameter in fuel modelling because most of the physical processes that occur in fuel elements during irradiation are thermally activated. The focus of this paper is the temperature distribution calculation used in the computer code ELESIM, developed at AECL to model the steady-state behaviour of CANDU fuel. A validation procedure for fuel codes is described and applied to ELESIM's thermal calculation. The effects of uncertainties in model parameters, like UO₂ thermal conductivity, and input variables, such as fuel element linear power, are accounted for through an uncertainty analysis using Response Surface and Monte Carlo techniques.

The magnitude of the fuel-to-sheath gap has a significant impact on fuel temperatures through its effect on the fuel-to-sheath heat transfer coefficient. Previous versions of ELESIM assumed a closed gap for the heat transfer coefficient calculation. While this is appropriate for most conditions typical for CANDU fuel and nominal pellet-to-sheath gap sizes, inclusion of a finite gap is necessary for low power situations or for gap sizes at the upper bound of the tolerance interval. For Light Water Reactor (LWR) fuel, "fragment relocation" is important to determining fuel-to-sheath heat transfer. The physical process proposed for fragment relocation is incomplete re-fitting of fuel pellet fragments caused by cracking during a thermal cycle, and it is typically modelled in LWR fuel codes with semi-empirical correlations. It has been suggested that the collapsible cladding for CANDU fuel would assure an almost permanent restraint on the pellet and prevent major fragment relocation. One of the goals of this study was to assess the possible need of a fragment relocation model for CANDU fuel.

To this end the latest developmental version of ELESIM, herein called ELESIM, includes a pellet eccentricity model for the fuel-to-sheath gap. When the gap is open the extent that the pellet is off-set from the sheath is considered a model parameter. By definition, full pellet off-set occurs when the pellet and the sheath are touching at one point for free-standing cladding, or at two diametrically opposed points for collapsible cladding. The typical condition for CANDU is collapsible, but large internal gas pressures can change the condition to free-standing.

To evaluate the pellet eccentricity model, ELESIM was used to simulate experiment FIO-142 with different options from a closed gap to a fully-eccentric gap. Experiment FIO-142 was a well-instrumented single element irradiation with measurements of both centerline temperature and neutron flux at two locations along the element.

The centerline temperature data from the FIO-142 experiment can also be used to validate ELESIM's temperature calculation. For the validation procedure, a unitless measure, ε , the relative difference between the calculated and measured values is used to qualify the agreement between calculations and measurements. Response Surface and Monte Carlo methods coupled with factorial design sampling techniques are used to create a simulated distribution of ε from knowledge of the uncertainties in the experimental conditions that are input variables for the code and in the measured values that are output variables for the code. By comparing the simulated ε distribution with the measured distribution it is possible to assess whether the discrepancies between measured and calculated data lie within the range expected from the uncertainties associated with the experiment and determine at the same time any systematic deviations of the models.

- 2. Simulation of the FIO-142 Test
- 2.1 Brief Description of the Experiment

Experiment FIO-142 consisted of a single fuel element irradiated in the NRU reactor in pressurized water coolant at a linear power of up to 55 kW/m for one operating cycle of 17 days. The fuel element was instrumented with thermocouples to measure sheath, end cap and upper and lower centerline fuel temperatures. The centerline fuel temperatures were measured with Type C thermocouples, while the remaining thermocouples used in the experiment were Type K, both having a precision of $\pm 1\%$ of the measured reading. Two flux detectors were also mounted on the fuel stringer.

Following irradiation, the fuel element was destructively examined with two sections of the element being analyzed for chemical burnup. Chemical burnup for the two sections was reported as 18.7 MWh/kgU and 20.6 MWh/kgU, with a measurement uncertainty of $\pm 5\%$ (2 σ).

2.2 Estimation of the Linear Power of the Experimental Fuel Element

The procedure for estimating the linear power of the fuel element is based on the assumption that the power is directly proportional to the flux detector readings (Equation 1) throughout the irradiation. In reality, the proportionality will change during the irradiation due to factors such as fission product buildup and plutonium disposition. Nevertheless, in the simulation of FIO-142, the proportionality is assumed to remain constant as the fuel element was irradiated to only a low burnup.

Therefore, the linear power, P, can be expressed in terms of a scaling factor, alpha, and the flux detector reading, R, as:

$$P = alpha * R$$
 (1)

The process used to determine the value of alpha is described below. In general, the burnup, Bu, is given by:

Bu(MWh/kgU) =
$$\frac{\int P(t) * conv * dt}{\pi * \rho * r^2 * (238/270)}$$
 (2)

where:

conv - unit conversion factor $(MW/1\times10^6 W) * (1000g/kg)$

ho - density of the UO₂ (g/cm³) r - fuel pellet radius (cm)

Using Equation (1) and replacing the integral in Equation (2) by the corresponding sum:

Bu (MWh/kgU) =
$$\frac{\text{alpha} * (RT) * \text{conv}}{\pi * \rho * r^2 * (238/270)}$$
 (3)

where RT is the sum of the product of flux detector readings and time intervals for the irradiation:

RT =
$$\sum_{i=1}^{n} \left(\frac{R1_{i,av} + R2_{i,av}}{2} \right) \left(\frac{\text{time}_{i} - \text{time}_{i-1}}{2} \right) \left(\frac{1}{3600} \right)$$
 (4)

and:

$$R1_{i,av} = \frac{R1_i + R1_{i-1}}{2}$$

$$R2_{i,av} = \frac{R2_i + R2_{i+1}}{2}$$

R1_i and R2_i are the ith readings for the two flux detectors.

Now, from Equations (2) and (3), alpha can be expressed in terms of burnup as

alpha =
$$\frac{Bu * \pi * \rho * r^{2} * \left(\frac{238}{270}\right)}{RT * conv}$$
 (5)

Since the chemical burnup is known at two positions in the fuel element, the corresponding values of alpha can be determined. The chemical burnup was determined by assuming an energy per fission for ²³⁵U of 200.8 MeV. The reported energy per fission for ²³⁵U in the NRX experimental reactor is about 185.0 MeV. While this value will vary among reactors, it is used in calculations for the NRU experimental reactor. As a result, the chemical burnup must be multiplied by the ratio (185/200.8) to correctly account for the burnup in the NRU reactor. Applying the ratio and accounting for the central hole, the following values of alpha were obtained:

Position (1) Burnup(1)=
$$18.7 \text{ MWh/kgU}$$
 alpha(1) = 843.4872

Position (2) Burnup(2)=
$$20.6 \text{ MWh/kgU}$$
 alpha(2) = 929.1831

Therefore, from Equation (1), the power histories at both locations in the fuel element can be estimated using alpha and the average flux readings for each history point.

The power history was reduced from more than 30,000 points to a more manageable number by averaging over eight hour intervals. Intervals were made smaller if the change in power was in excess of 2 kW/m from one step to the next. The measured centerline temperatures corresponding to the averaged power in each interval were also recorded. This resulted in a power history of just 136 steps, and a data set of 136 corresponding fuel centerline temperature measurements. The power histories resulting from this "condensing" process were used to complete an ELESIM input file for FIO-142. The geometry data used in the input file came from the fabrication report for this test element.

2.3 Simulation Results

ELESIM test cases were created to account for different fuel-to-sheath gap conditions. All power histories were simulated for (a) an open, concentric gap, (b) an open, eccentric gap, and (c) a closed gap. In terms of fragment relocation models used for LWR fuel, case (a) corresponds to no relocated fuel fragments, case (b) corresponds to partial relocation, while case (c) corresponds to 100% relocated fuel fragments.

An initial comparison revealed that the measured and calculated results agreed reasonably well except during times when the flux (and hence power) was changing rapidly. It was concluded that this discrepancy was due to the response time of the flux detectors (the rhodium flux detectors have a response time of about 5 min), rather than the performance of the code and the decision was made to reject data points that occurred during periods when the flux was changing rapidly i.e. during power ramps and shut downs.

For the open concentric fuel-to-sheath gap (case (a)), the calculated centerline temperatures follow the measured temperature trends throughout the irradiation for both power histories. For the first power history (Figure 1), the calculated temperatures are higher than measured with an average difference between calculated and measured temperatures of 47 K. The second power history (Figure 2) also results in temperatures that are higher than measured with an average difference of 67 K. For both power histories, the fuel-to-sheath gap is calculated to be open for most of the irradiation, resulting in a low fuel-to-sheath heat transfer and higher fuel temperatures. In

addition, the difference between measured and calculated temperatures increased with time at power for both histories.

The calculated temperatures for case (b), the open eccentric gap (Figures 3 and 4), show better agreement with the measured temperatures for both power histories. The average difference between calculated and measured temperatures is 27 K for the first power history. The calculated temperatures are slightly higher than measured for the second power history with an average temperature difference of 37 K. As for the open concentric gap case, the fuel-to-sheath gap is calculated to be open for most of the irradiation history. However, the gap is smaller resulting in better agreement between calculated and measured temperatures relative to case (a). For the second power history, Figure 4 shows the difference between calculated and measured temperatures to be increasing with time at power.

For the closed gap case, the calculated centerline temperatures are lower than the measured values for most of the irradiation (Figures 5 and 6). The average temperature difference for both power histories is about 47 K. For the closed gap option, ELESIM Mod11 calculates the fuel-to-sheath heat transfer coefficient for a closed fuel-to-sheath gap, even if the gap may be open. This results in a higher heat transfer coefficient and lower fuel temperatures relative to the other gap cases. As seen in the other simulations, the difference between calculated and measured temperatures increases with time for both power histories.

The increasing difference between calculated and measured temperatures over time likely indicates that the scaling factor, alpha, used in the power estimation may not be constant throughout the irradiation as originally assumed. To account for this, the FIO-142 power histories should be generated by a reactor physics code to include the effects of fission product buildup and plutonium disposition in the fuel.

The uncertainty on the measured chemical burnup was estimated to be $\pm 5\%$, which translates directly to a $\pm 5\%$ uncertainty in the estimated power. To investigate the effect on calculations, several of the ELESIM simulations were rerun using power histories that were modified by $\pm 5\%$. Note that only the power history corresponding to the lower burnup was used for these simulations.

Figure 7 compares the calculated centerline temperatures for the original and the $\pm 5\%$ power histories with the measured temperatures for the open eccentric gap case. Changing the power history by $\pm 5\%$ results in calculated temperatures that bracket the measured temperature.

For the closed gap, the calculated temperatures were slightly lower than measured throughout the irradiation. Therefore, the simulation was rerun using a power history that was increased by 5%. This resulted in temperatures that are slightly higher than measured in the first half of the irradiation, and in good agreement with measured thereafter (Figure 8).

These initial temperature comparisons did not take into account other uncertainties associated with the models used to calculate the fuel temperatures. If these uncertainties can be properly included, our confidence in the agreement between the measured and calculated temperatures for the estimated power histories improves. To account for uncertainties in measured values of both input and output parameters, we are proposing a validation methodology that investigates the differences between a set of experimental data and the corresponding code calculations. If both the experiment and code were perfect, the differences would be zero. In fact, there are uncertainties in the experimental results which are stochastic in nature, and we expect the differences between calculated and measured values to be non-zero, but distributed around the zero value. That is, we expect the mean of the differences to be zero. In addition, the models implemented in the code rely on approximations and idealizations, and can contain mistakes that induce systematic errors. If the code has a tendency to over- or under-predict, the mean of the differences will not be zero. Therefore, one requirement for validation is that this mean must be less than a specified value.

It is possible that the code both over- and under- predicts values for the set of validation data. In this case, the mean of the differences between the calculated values and measured values may be close to zero. Therefore, it is not sufficient for the mean to be close to zero to consider the code validated. The differences must be further analyzed

in terms of the distribution around the mean. Our proposed technique assesses the response of the code to uncertainties in the experimental and input data, and this information is used to predict the variance in the differences between measured and calculated values. If the code is accurately simulating the behavior of the relevant physical phenomena, the predicted variance between the measured and calculated values should match the observed variance. If the predicted variance is less than the observed variance, there are differences between the calculated and measured results that can not be explained by uncertainties in the experimental conditions and input values.

The following section outlines a validation exercise based on our proposed technique. The pellet eccentricity option has proven to give the most satisfactory results, and consequently was chosen for the validation exercise.

3. The Validation Procedure

The complete validation procedure is outlined in this section as a series of steps.

- 1) A suitable validation data set is identified and the corresponding code simulations are performed.
- The code simulations are compared to the validation data using the dimensionless parameter, ε. The ε values are calculated according to:

$$\varepsilon_i = \frac{y_i^c - y_i^m}{y_i^m} \tag{6}$$

where, y_i^c , is a calculated value and y_i^m , is the corresponding measured value.

- The frequency distribution of the ε values is plotted and the mean value of ε is examined. If this is greater than a specified maximum value, the code results and the experimental results disagree, i.e., the code fails the validation exercise.
- 4) Uncertainties are assigned to each input parameter of the code, including parameters that describe the experimental conditions (the descriptive parameters), material data, model parameters and other input data that characterize the test materials.
- The response of the code is sampled around each data point, with a variance on each input parameter using a Plackett and Burman two level experimental design.
- A linear response surface is fitted to the response values.
- 7) Backwards elimination is used to determine which of the input parameters contribute to the response of the code.
- 8) The code is sampled in greater detail with variances only on the reduced parameter set determined in step 7.
- 9) A combination of forward selection and backwards elimination is used to fit a second order response surface to the new sampled code results.
- The fit of the response surface is checked by re-sampling the code, and the response surface is modified if necessary.

- The frequency distribution calculated from the code response and the distribution associated with the uncertainty in the experimental measurements of the output parameters are combined by Monte Carlo sampling to produce a theoretical distribution for ε .
- 12) The theoretical variance in ε is compared with the observed variance in ε. If the theoretical value is greater than the observed value, any discrepancy between the code and the experimental data can be explained by uncertainties in the input parameters and the code can be said to be valid.

4. Validation Exercise for FIO-142

In this validation exercise, each time step calculated by the code was treated as an independent experiment and a response surface was required for each time step. Rather than carry out the complete response surface fitting for each time step, it was expected that the general form of the response surface would be the same for every data point, meaning that a complete stepwise regression analysis was only required for one point. Once the general form of the response surface had been determined, it was easy to fit the general form to the actual sampled code response at each time step by least squares. The final result was a series of response surfaces, all with the same form, but individually fitted to the code response at each time step. The time at the end of the tenth time step was chosen for the determination of the general form of the response surface.

4.1 Computation of ε

The measured temperatures and corresponding calculated values were used to calculate the dimensionless parameter ε in accordance with equation (6). The resulting values are plotted in Figure 9.

4.2 Calculation of the Frequency Distribution of ε

Once the ε values had been found, the frequency distribution was determined and plotted. The range of values was divided into 10 equal intervals (or bins) and the number of ε values contained by each interval was counted. The counts were normalized to the total number of data points and the resulting frequency distribution plotted, Figure 10. The mean value of the distribution is 0.008 or 0.8% which can be interpreted as indicating a very good match between the calculated and measured data. The spread of the distribution is characterized by the standard deviation which in this case is 0.031 or 3%.

4.3 Uncertainties in the Input Parameters

The next step was to assign uncertainty distributions to the code input parameters. For this exercise only ten input parameters of the ELESIM code were chosen for study, based on expert judgement and previous knowledge of fuel behaviour (Table 1). At this stage only the extreme limits of the uncertainty ranges for each parameter were required. Note that ELESIM includes input parameters that allow for the adjustment of the power history and UO₂ thermal conductivity through scaling factors. The ten input parameters include 1) parameters that have an influence on the centerline temperature, and 2) parameters that were thought to have no (or very little) effect on the fuel temperature. The latter were included to illustrate the ability of the regression fitting process to identify which parameters are necessary for the analysis and which may be rejected from the study.

4.4 Initial Sampling of the Code Response

The first stage of fitting the response surface required sampling the response of the code so that the effects of the individual parameters could be distinguished in the following regression analysis. This was achieved by using a Plackett and Burman, two level experimental design for the ten chosen parameters. Plackett and Burman supply optimized experimental designs which involve N simulations for values of N up to 100. Two restrictions apply: 1) N must be a multiple of four, and 2) N must be greater than the number of parameters being studied. In this exercise with ten parameters, the design for N=12 would have been adequate. However, the design with N=16 was chosen as it reduced the effects of second order confounding without overly increasing the computational effort.

The two levels used for each parameter were the extremes of the range of uncertainties given in Table 1. The sampling matrix is shown in Table 2, where a - or + sign indicates that a parameter has been assigned the lower or upper limit of its uncertainty range, respectively.

4.5 Fitting of the Linear Response Surface

Following this initial sampling, a linear response surface was least squares fitted to the sampled data. The linear response surface initially contained all 10 of the input parameters in the study and was of the form:

$$y = \beta_0 + \beta_1 x_1 + \beta_2 x_2 + \dots + \beta_{10} x_{10}$$
 (7)

4.6 Backward Stepwise Regression

Backward stepwise regression was used to eliminate those parameters that did not significantly contribute to the fit of the regression surface. A measure of the contribution to the fit of a given input parameter is, t, the absolute value of the ratio of the corresponding coefficient in relation (7) to its standard deviation [1]. The parameter with the minimum t ratio was rejected if that t ratio was less than 2. At this first step parameter 10, the sheath thickness, had the smallest t ratio (and it was less than 2) so it was rejected and the surface was fitted to the remaining nine parameters. Removing parameters from the regression surface has the effect of changing both the β coefficients and t ratios of the remaining parameters. After four more steps, the minimum t ratio calculated was greater than 2 signifying that the remaining five parameters significantly contributed to the fit of the response surface. The remaining five parameters with β coefficients and t ratios are shown in Table 3. Also shown in Table 3 is the coefficient of multiple determination R^2 =99% for this first stage linear response surface fitted to the sixteen sampled points of the Plackett and Burman design.

4.7 Second Stage Sampling of the Code

The fitting of the linear response surface to the first stage sampling of the code allowed the parameter set to be reduced to five parameters. Therefore, a second-order fit was achieved with a full two level factorial design with just 32 code simulations. To provide the additional information required to uniquely determine the quadratic terms, 5 additional code simulations were conducted. In these five new tests one parameter at a time was varied from the nominal values, to generate an additional data point along each axis in the parameter space.

4.8 Fitting of the Second Order Response Surface

To fit the second order response surface to the results of the second stage experimental design, a combination of forward selection and backward elimination was used. The first step was to fit the linear terms of the five parameters to the 37 results of the factorial design and the result of the nominal run. As the response surface would be Monte Carlo sampled around the nominal value, it was clear that the response surface should be "forced" to pass through the nominal code result. This was achieved by use of a simple coordinate transformation to make the origin of the parameter space correspond to the nominal value.

The coefficients were again determined by a least squares fit and as before, the t ratios were calculated. The next stage was to add the higher order terms using forward selection and backwards elimination. The higher order terms were tried one at a time in the regression surface and either accepted or rejected based on the corresponding t ratio. In some cases, the addition of a term caused the t ratio of an existing term to fall below 2. This implied that either of the parameters, but not both, should be included in the response surface. When such a situation arose, the term with the larger t value was retained. After all the terms of the second order equation had been tested and rejected or retained, a nine term response surface remained with a coefficient of multiple determination of 98%.

In an attempt to improve the fit of the response surface, some of the terms that had been initially rejected but had t ratios that came close to 2 were retried in the response surface. It is interesting to note that on trying these terms again, after additional terms had been added to the response surface, they showed increased t ratios. Finally, a 12

term response surface was settled upon and the β values and t ratios are shown in Table 4. This response surface has a coefficient of multiple determination of 98.7%. Although the t ratios of the last two terms are less than two, and they contribute little to the fit of the response surface, it was decided to keep these within the response surface as the additional computational effort involved in the following steps would be very small.

The final stage was to generate the complete set of response surfaces by linear least squares fits to the data for each time step.

4.9 Testing the Response Surface

The coefficient of multiple determination, R², is a measure of the amount of variation in the sampled data that is explained by the response surface. In the generation of the response surface, the majority of the code samples were taken at the extremes of the expected ranges of the input parameters. The R² calculated from these samples need not necessarily be a good measure of the match between the response surface and the true code response at intermediate values. In order to test the match at intermediate values of the input parameters, ten further samples were taken of the code response. As both the fit of the response surface achieved in step 9 and the selection of parameters from step 7 were to be tested, all ten of the parameters identified in step 4 were included in the sampling. The values of the input parameters were assigned with a random number generator and scaled to provide values between the identified extreme ranges for each parameter.

The sampled values were compared with calculations made with the response surfaces and R^2 was found to be 99.4%. While this high value for R^2 indicates that the overlying trend of the sampled data is well matched by the response surfaces, it does not give a good indication of local deviations. To investigate local deviations, the percentage error between the sampled data and the response surface was calculated at each time step for each of the sample simulations. The average absolute percentage differences indicate that the difference between the response surfaces and the code response is typically $\sim 1.7\%$, but has a maximum value of 10%.

There is the temptation to include the code results used for this testing of the response surfaces in the fitting of additional higher order terms. This should be avoided as the addition of these samples will weight the fit of the response surface around the test points and give misleading information on the accuracy of the fit achieved.

4.10 Monte Carlo Sampling of the Response Surface

The next stage in the exercise was the determination of the theoretical distribution of ε_i by Monte Carlo sampling of the response surface. The measured ε_i values are given by relation (6). The theoretical distribution of ε_i was determined by Monte Carlo sampling the distributions of the measured and calculated values. The former is the best estimate of the uncertainty in the direct measurement of y_i^m , while the latter is determined by sampling the code response to uncertainties in the input.

4.11 Comparison of the Theoretical and Measured Frequency Distributions of ε

Having completed the calculation of a theoretical set of ϵ values, the theoretical frequency distribution of ϵ was plotted in the same manner as described in step 3. Figure 11 shows a graph of both the theoretical and measured distributions. It is readily apparent from the graph that the theoretical distribution straddles the measured distribution indicating that the differences between the code calculated and measured values can be explained as uncertainty in the input parameters. This is further supported by the values for the variances of the distributions:

$$\sigma_{th} = 0.05$$
 and $\sigma_{cm} = 0.03$

 $\sigma_{th}^2 > \sigma_{cm}^2$ fulfills the validation criteria. Therefore, the fuel centerline temperature calculations of ELESIM have been successfully validated against the experimental data. The minimum uncertainty that can be quoted for the fuel centerline temperature is a variance of 5% (based on $\sigma_{th} = .05$).

5. Conclusions

Experiment FIO-142 has been simulated using ELESIM. The power histories used in the simulation have been estimated from the flux detector readings and the chemical burnup at two locations in the fuel element. Simulation results show both closed and open fuel-to-sheath gap models in ELESIM capture the trends in measured temperature behaviour. The temperatures for a closed gap are slightly lower than the measured temperatures throughout the irradiation. The temperatures for an open eccentric gap are in good agreement with the measured values, and the temperatures for an open concentric gap are slightly higher than measured. Since the closed gap model corresponding to 100% relocated fuel fragments does not provide the best agreement, it is unlikely that a fuel fragmentation model is required for CANDU fuel.

A trend of increasing difference between the calculated and measured temperatures over time was seen for most simulations. This indicates that the scaling factor used in the power estimation may not be constant throughout the irradiation as originally assumed. Therefore, the FIO-142 power histories should be generated by a reactor physics code to account for the effect of fission product buildup and plutonium buildup and disposition in the fuel.

The thermal module of ELESIM code was subjected to a validation procedure and shown to meet the two validation conditions identified in the procedure said to be validated within the uncertainty of the predicted variance, 5%. Included in this variance are all the uncertainties in the input values and the experimental procedures used in the generation of the validation data. This variance represents the current state of knowledge of the uncertainty of the code and is the least uncertainty that may be applied to a code calculation.

It should be stressed that this is not the uncertainty that may be quoted for other applications of the code. Clearly other code applications may involve greater uncertainties in the input parameters than those involved in the validation exercise. Every application of the code requires its own uncertainty analysis. This validation exercise has only placed a lower limit on the possible uncertainty of a code simulation.

REFERENCES

- [1] Box G.E.P, and Draper N.R., "Empirical Model-Building and Response Surfaces". J. Wiley & Sons. 1987. ISBN 0-471-81033-9.
- [2] Plackett R.L., and Burman J.P., "The Design of Optimum Multifactorial Experiments". Biometrika, 33, 305-325 and 328-332. 1946.

Number	Parameter	+	-
1	Power	+5%	-5%
2	Pellet / Sheath Gap (mm)	0.15	0.05
3	Thermal Conductivity of UO ₂	+15%	-15%
4	Fill Gas Volume	+40%	-40%
5	Roughness of Pellet (µm)	3.0	0.5
6	Roughness of Sheath (µm)	1.4	0.8
7	Grain Size (μm)	30	7
8	Dish Depth (mm)	0.25	0.18
9	Density of Pellet (Mg/m³)	10.8	10.4
10	Sheath Thickness (mm)	0.45	0.38

Table 1. Ranges of the ten initial input parameters.

Sample	Input									
	1	2	3	4	5	6	7	8	9	10
1	+	_		-	+	-	-	+	+	-
2	+	+	-	-	-	+	-		+	+
3	+	+	+	-	-	-	+	-	_	+
4	+	+	+	+	-	-	-	+	_	-
5	-	+	+	+	+	-	-	-	+	-
6	+	-	+	+	+	+	-	-	_	+
7	-	+	-	+	+	+	+	-		-
8	+	-	+	-	+	+	+	+	-	-
9	+	+	-	+	-	+	+	+	+	-
10	-	+	+	-	+	-	+	+	+	+
11	_	-	+	+	-	+	-	+	+	+
12	+	_	-	+	+	-	+	-	+	+
13	-	+	-	-	+	+	-	+	-	+
14	-	-	+	-	-	+	+	-	+	-
15	-	-	-	+	-	-	+	+	-	+
16	-	-	-	-	-	-	-	-	-	-

Table 2. The Plackett and Burman sampling matrix.

Parameter	t ratio	beta	R squared
0	7.967022	2475.528	0.986737
1	8.006105	9.375833	
2	7.7487	907.439	
3	24.37161	-9.51375	
5	3.29679	15.44329	
9	3.871562	-113.348	

Table 3. The coefficients of the remaining five parameters at the end of the fitting of the linear response surface.

Parameter	t ratio	beta	R squared
1	12.08267	1087.722	0.986736
2	7.165223	721.2384	
3	30.25039	-908.9	
5	3.161279	10.18684	
9	10.94431	-219.42	
X ₂ ²	7.00198	-1061.38	
X ₃ ²	8.683666	2107.001	
X_1X_2	3.739828	-2017.3	
X ₃ X ₉	3.183308	428.9158	
X ₂ X ₅	2.27098	146.9969	
X ₁ X ₉	1.737267	-702.145	
X ₂ X ₃	1.53563	828.3301	

Table 4. The final twelve term response surface.

	Parameter	Type	mean	sigma	range
1	Power	Normal	1	2.5%	-
2	Radial gap	Square	0.102	-	0.082-0.122
3	UO ₂ thermal conductivity	Normal	1	7.5%	-
5	Pellet Roughness	Square	0.81	-	0.65-0.97
9	Pellet Density	Square	10.7	-	10.6-10.8
Output	Fuel Centerline Temperature	Normal	y _i °	3.3%	-

Table 5. Distributions assigned to the five parameters for Monte Carlo sampling.

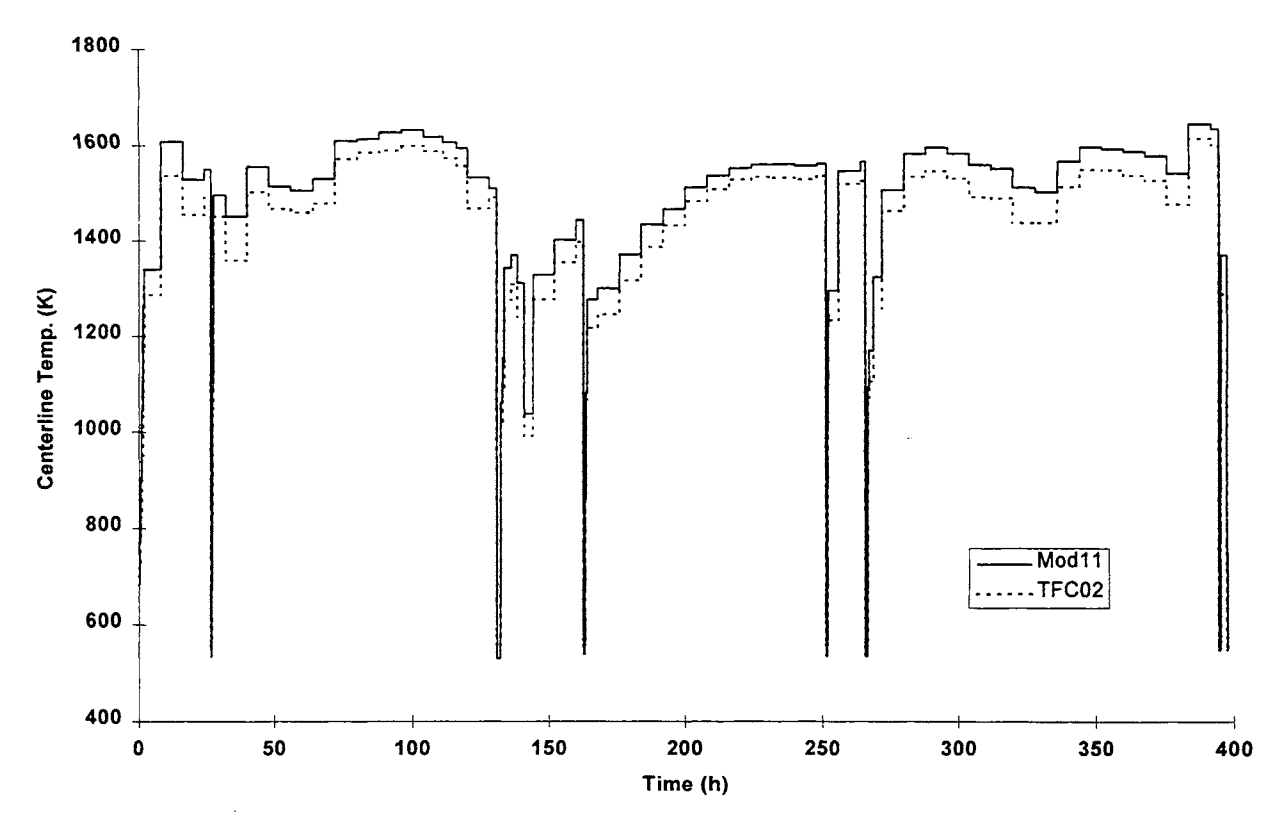


Figure 1 Centerline Temperature vs. Time for First Power History, Open Concentric Gap

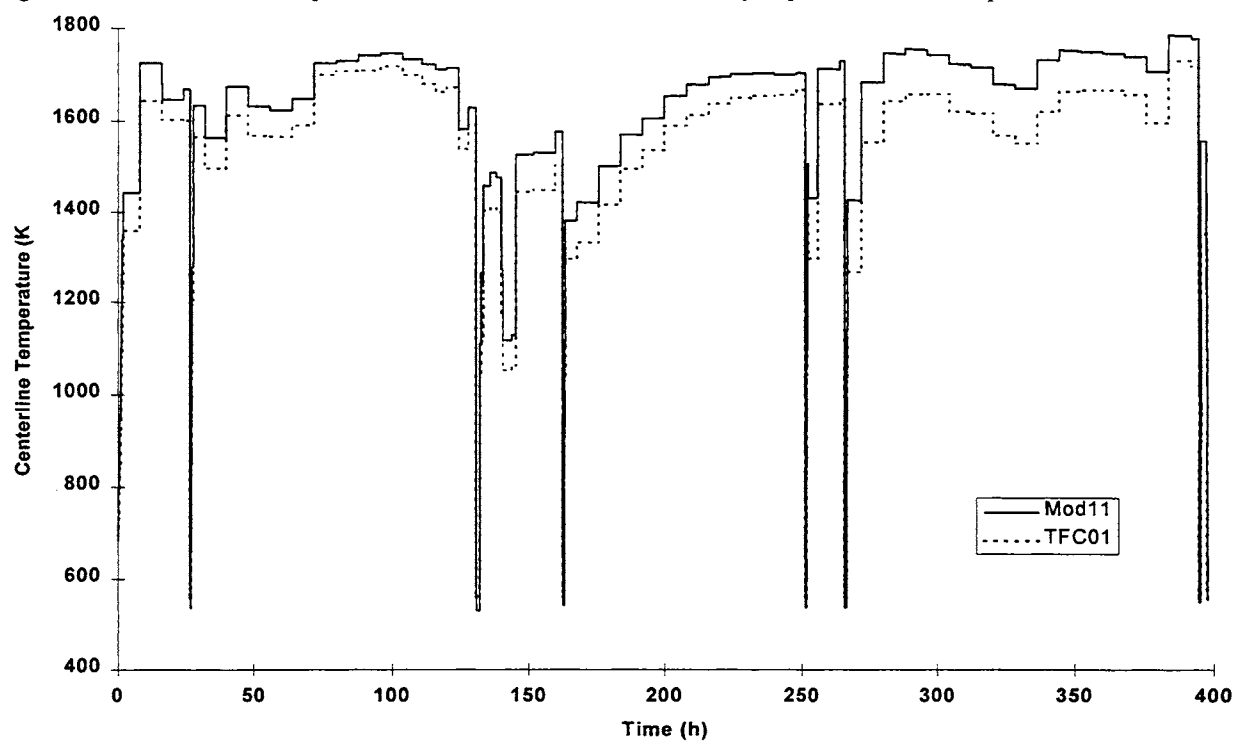


Figure 2 Centerline Temperature vs. Time for Second Power History, Open Concentric Gap

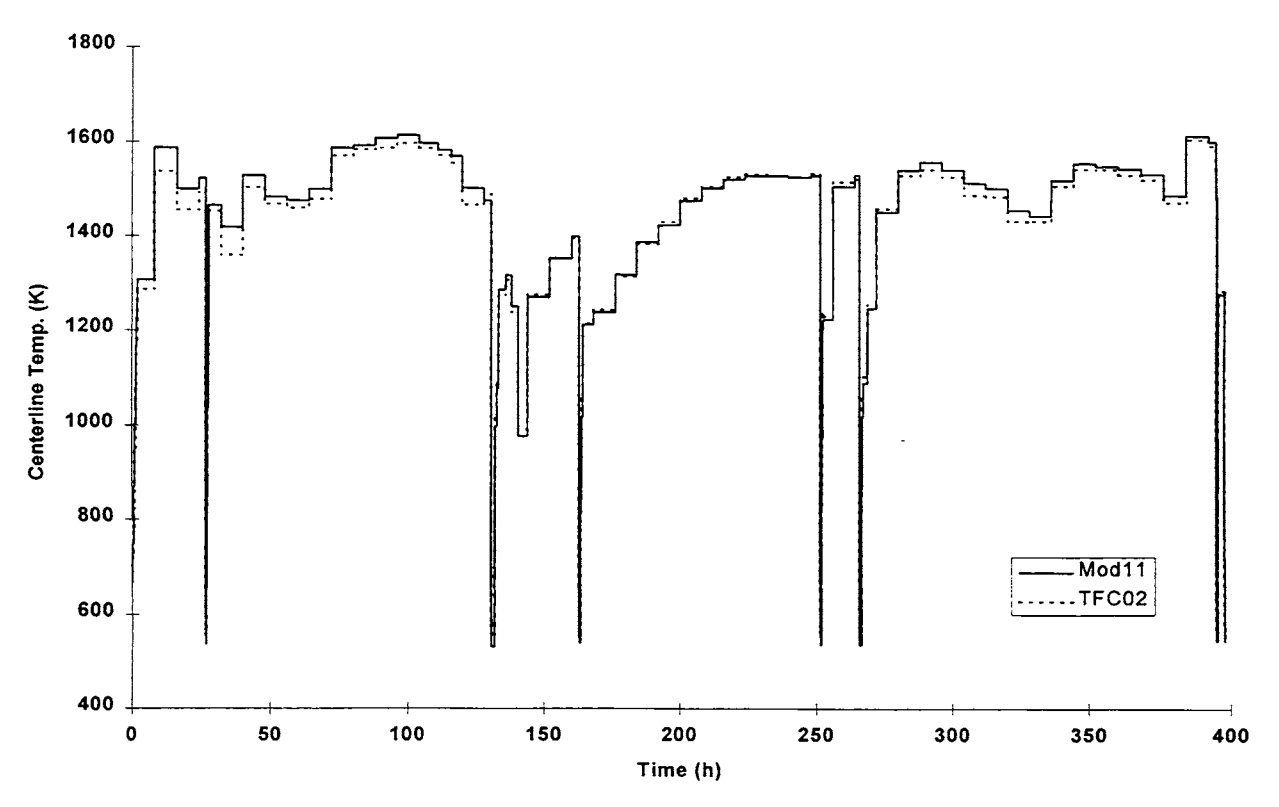


Figure 3 Centerline Temperature vs. Time for First Power History, Open Eccentric Gap

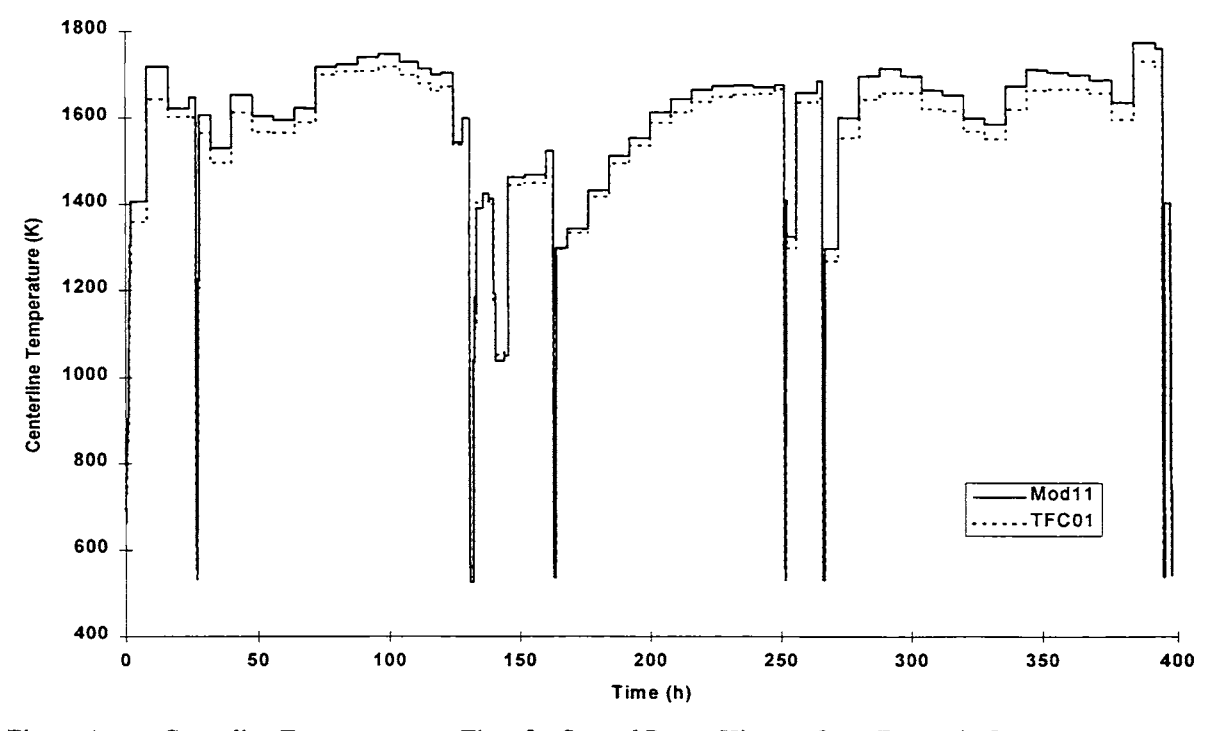


Figure 4 Centerline Temperature vs. Time for Second Power History, Open Eccentric Gap

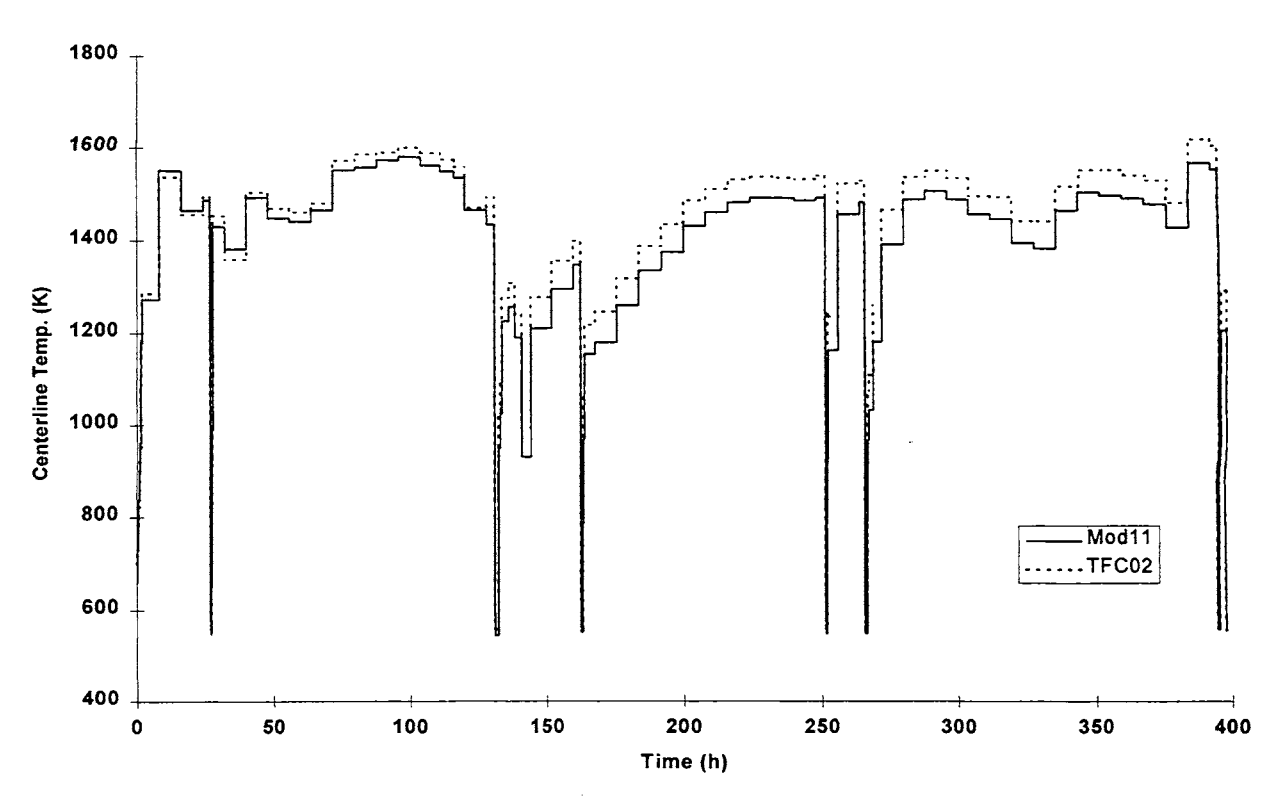


Figure 5 Centerline Temperature vs. Time for First Power History, Closed Gap

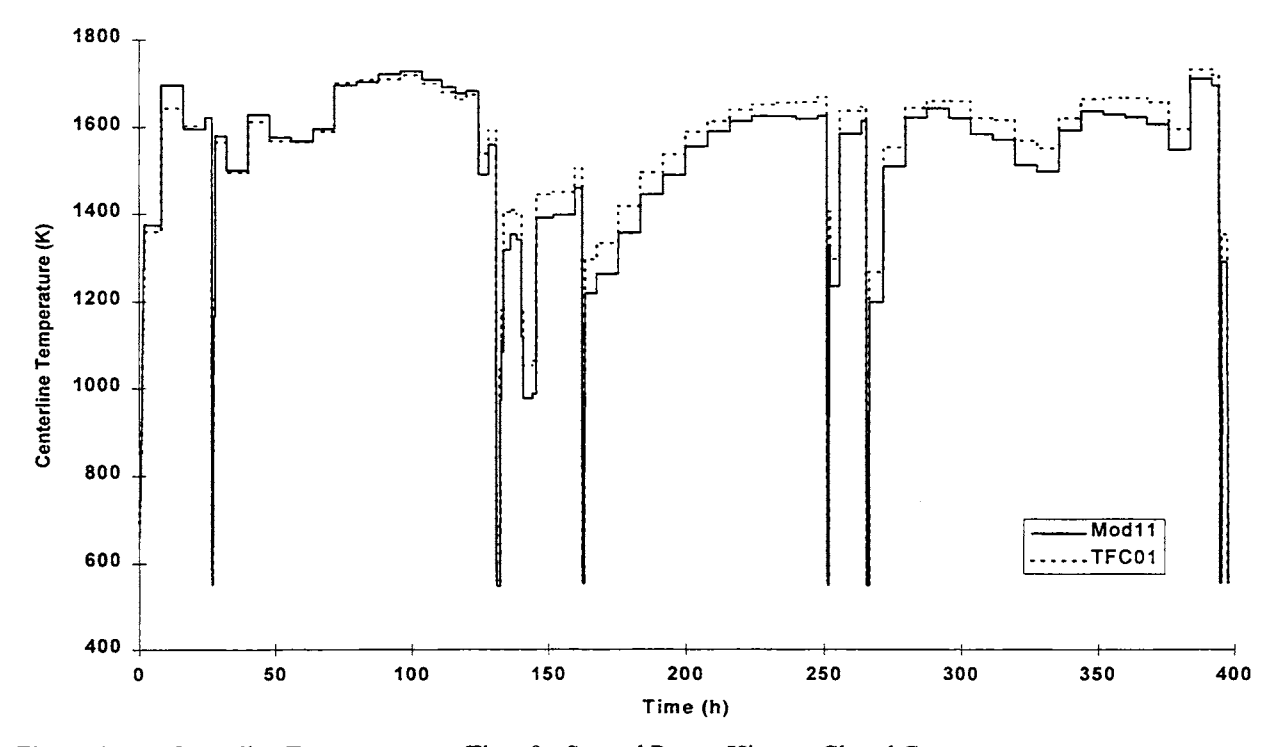


Figure 6 Centerline Temperature vs. Time for Second Power History, Closed Gap

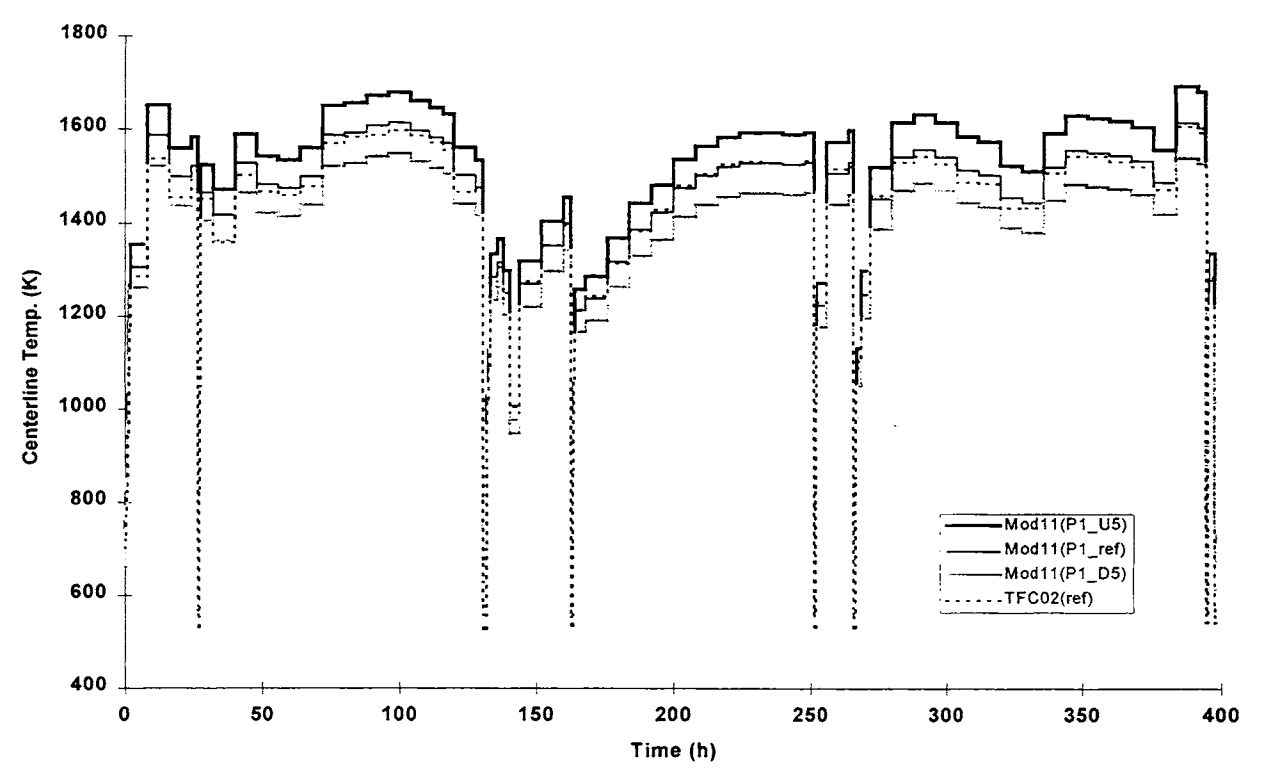


Figure 7 Centerline Temperature vs. Time for Second Power History, Power Varied by ±5%, Open Eccentric Gap

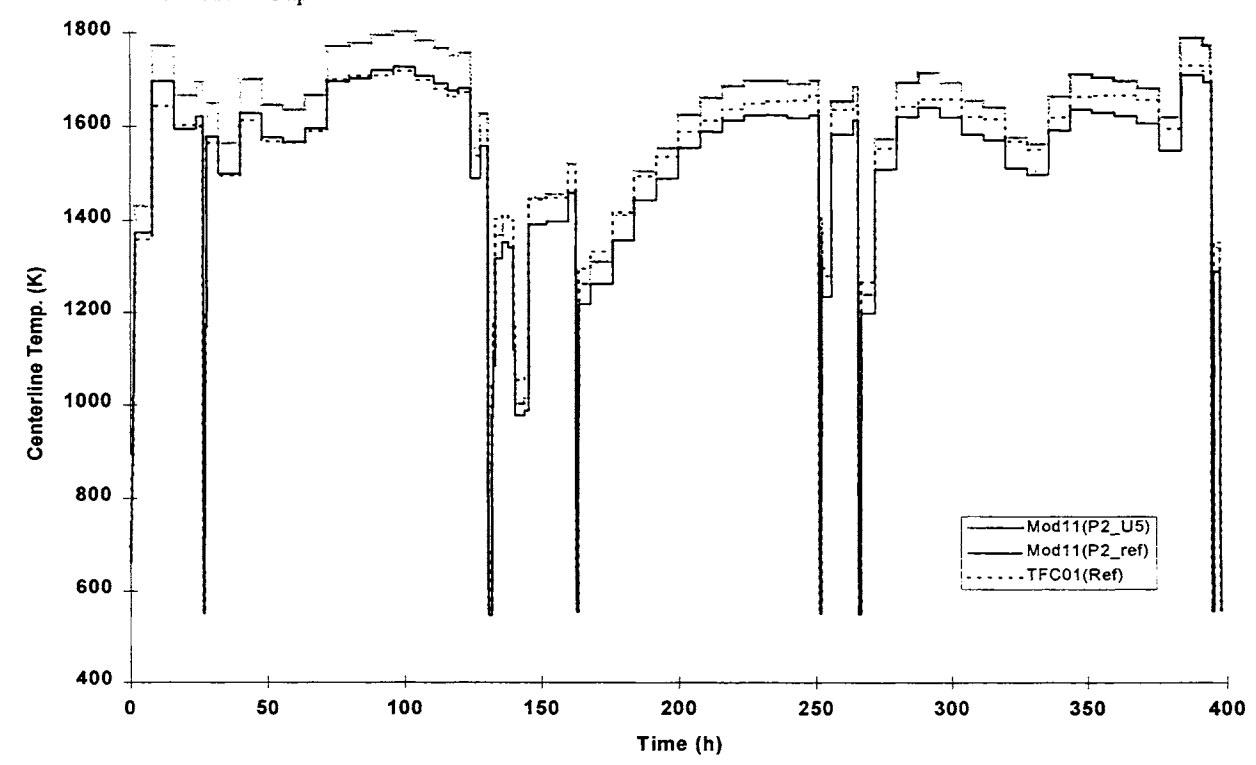


Figure 8 Centerline Temperature vs. Time for Second Power History, Power Increased 5%, Closed Gap

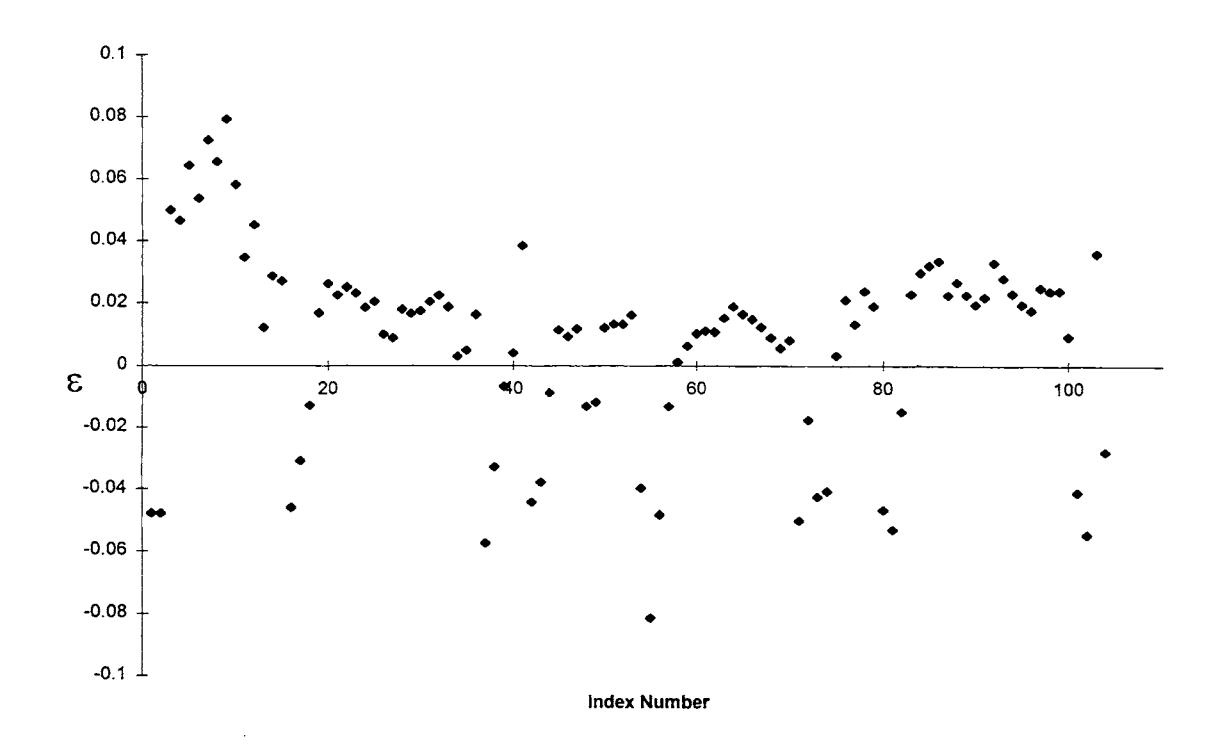


Figure 9. ϵ values for the example validation exercise

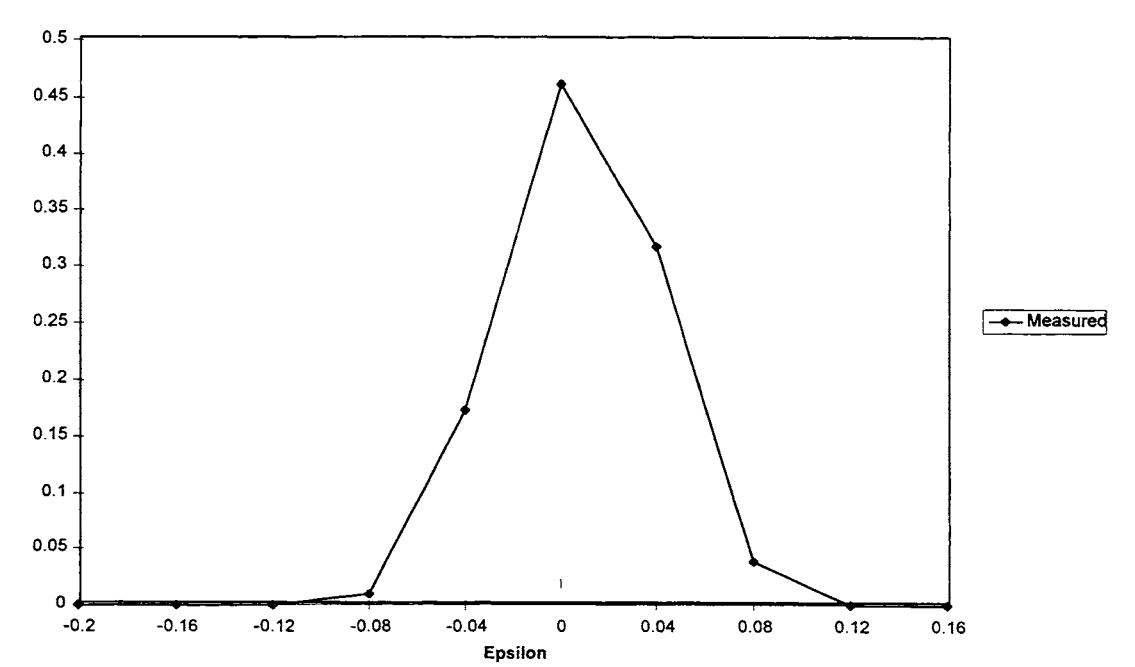


Figure 10. The measured frequency versus ϵ distribution.

Theoretical and Measured Epsilon Distributions

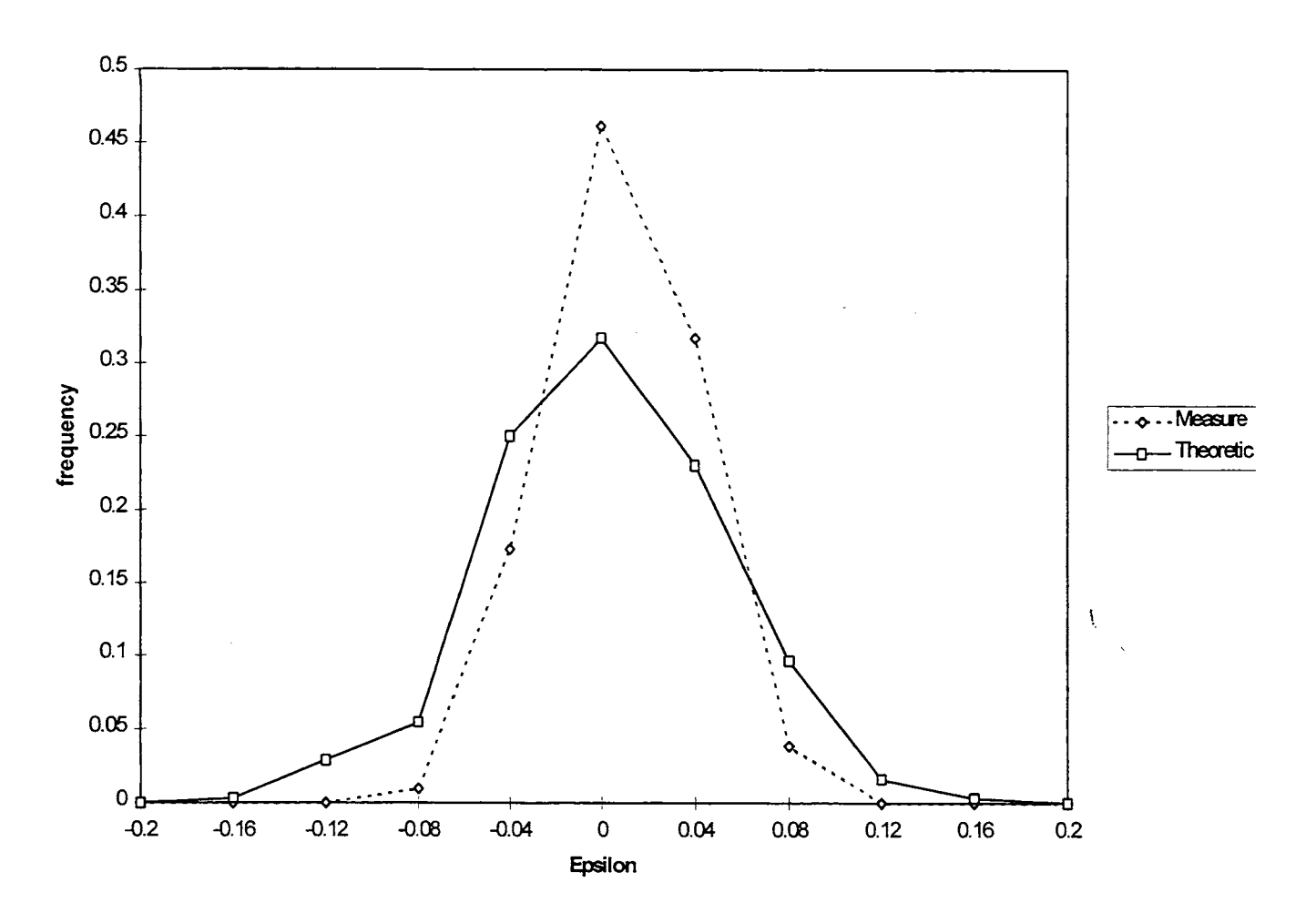


Figure 11. The theoretical and measured ϵ distribution.